Toxicology Research

PAPER

Cite this: *Toxicol. Res.*, 2015, **4**, 351

# Mitochondrial dysfunction and oxidative damage in the liver and kidney of rats following exposure to copper nanoparticles for five consecutive days†

Ronghui Lei,‡[a,b] Baohua Yang,‡[a] Chunqi Wu,[a] Mingyang Liao,[a] Rigao Ding[a] and Quanjun Wang*[a]

*Objective*: The goal of the current study was to investigate the molecular mechanisms of copper nanoparticle (CuNP)-induced hepato- and nephrotoxicity by a proteomic analysis that was phenotypically anchored to conventional toxicological outcomes. *Methods*: We employed specialized proteomic techniques, namely two-dimensional difference gel electrophoresis coupled with mass spectrometry to analyze the changes in protein expression in rat liver and kidney after 5 days of oral copper nanoparticle administration. Serum biochemical analyses and histopathological examinations of livers and kidneys of all rats were also performed. *Results*: All of the results indicated that the adverse effects observed in the rats treated with 100 mg $kg^{-1}$ $d^{-1}$ nanocopper were less than those induced by 200 mg $kg^{-1}$ $d^{-1}$ CuNPs. Exposure to CuNPs at a dose of 200 mg $kg^{-1}$ $d^{-1}$ for 5 d can induce overt hepatotoxicity and nephrotoxicity through a mechanism that mainly involves scattered dot hepatocytic necrosis and widespread renal proximal tubule necrosis. In addition, significantly elevated copper accumulation, decreased thiol groups and elevated malondialdehyde levels were also observed in the liver and kidney tissues. The perturbed proteins identified in the rat livers and kidneys are mainly involved in the respiratory and energy metabolisms, antioxidant defense, phase II metabolism, lipid metabolism, urea cycle, creatine biosynthesis, intracellular calcium homeostasis, and cytoskeletal organization. No abnormalities were identified in the liver and kidney tissues from the rats treated with 200 mg $kg^{-1}$ microcopper. *Conclusions*: The results of this study suggest that mitochondrial dysfunction and oxidative damage may be the initial events in the hepato- and nephrotoxicity of copper nanoparticles. The down-regulation of phase II metabolic enzymes in the liver and the decrease in calcium-binding proteins in the kidney appear to be specific modes of action in these target organs. Our findings offer new directions for future research aiming to identify the specific biomarkers of the hepatotoxicity and nephrotoxicity of copper nanoparticles.

Received 30th September 2014,
Accepted 12th December 2014

DOI: 10.1039/c4tx00156g

www.rsc.org/toxicology



## Introduction

Copper nanoparticles (CuNPs) are among the most important engineered nanoparticles. Because of their excellent optical, electrical, catalytic, and antimicrobial properties, they are widely used in electronics, ceramics, films, polymers, inks, metallics, lubricant oils, and coatings.[1,2] In addition, CuNPs have shown great promise in the development of antibacterial products, as a supplement in livestock and poultry feed, and as a component of intrauterine contraceptive devices.[3] The increase in CuNP production and application increases the likelihood of the release of CuNPs into the natural environment and thus of human exposure to these particles. Previous research has demonstrated that CuNP exposure produces hepatotoxicity, nephrotoxicity, and heavy splenic injury in experimental rats and mice[3,4] and gill toxicity in zebra fish.[5] Additionally, the results of *in vitro* comet assays and trypan blue staining suggest that CuNPs cause DNA damage and cytotoxicity.[6] Although the toxic effects and mechanisms of CuNP exposure have been studied *in vivo* and *in vitro*,[7–10] the toxic mechanisms of CuNPs—an understanding of which is important for assessing human health and the environmental impacts of CuNPs—still need further investigation.

The integration of traditional toxicology approaches with transcriptomic, proteomic, and/or metabolomic analyses has

[a]*State Key Laboratory of Toxicology and Medical Countermeasures, Institute of Pharmacology and Toxicology, Academy of Military Medical Sciences, 27 Taiping Road, Beijing, 100850, P. R. China. E-mail: wangquanjunbeijing@163.com*
[b]*School of Public Health, Health Science Center of Xi'an Jiaotong University, Xi'an, Shanxi, P. R. China*
†Electronic supplementary information (ESI) available. See DOI: 10.1039/c4tx00156g
‡Ronghui Lei and BaohuaYang have contributed equally to this work.

been used to elucidate the modes of action of various toxicants and gain new insights into the adverse effects at the molecular level.[11] The challenge of this discipline, called systems biology, is to integrate data from different platforms with their advantages and limitations.[12] Previous studies incorporating metabolomics and transcriptomics have revealed that mitochondrial failure, enhanced ketogenesis, fatty acid β-oxidation, and glycolysis contribute to hepato- and nephrotoxicity in male rats orally administered CuNPs (200 mg $kg^{-1}$ $d^{-1}$) for five days. The triglyceride level in the serum, liver, and kidney may serve as a sensitive biomarker for CuNP-induced lipidosis.[3] Significant alterations in the expression of many genes involved in valine, leucine, and isoleucine degradation, complement and coagulation cascades, oxidative phosphorylation, cell cycle, mitogen-activated protein kinase signaling pathway, glutathione metabolism, and other pathways have been reported in rats following CuNP administration, and these changes may be related to the development of hepato- and nephrotoxicity.[13,14]

In the current work, we present liver and kidney proteomics data for the hepato- and nephrotoxicity induced after exposure to CuNPs. The protein modulations were evaluated by two-dimensional difference gel electrophoresis (2D-DIGE) followed by mass spectrometry identification. The aim of this work was to provide new insights into CuNP-induced hepato- and nephrotoxicity through a combination of proteomic and traditional toxicological analyses.

## Materials and methods

### Materials

Commercial-grade CuNPs (25 nm) were purchased from Shenzhen Zunye Nano Material Co. Ltd (Shenzhen, China). Copper microparticles (CuMPs 200-mesh) were purchased from Beijing HaoYun Industry Co. Ltd (Beijing, China). The CuNPs and CuMPs were suspended in a 1% (w/v) HPMC solution (K4M, Shanghai Colorcon Coating Technology Ltd, Shanghai, China). The CuNP and CuMP suspensions were prepared as described previously.[4] The protease inhibitor cocktail used was purchased from Roche (Basel, Switzerland). Molecular-weight markers were obtained from Amersham Biosciences (Little Chalfont, UK). The cyanine dyes Cy2, Cy3, and Cy5 were purchased from Amersham Biosciences (Little Chalfont, UK), and ReadyStrip™ immobilized pH gradient (IPG) strips (17 cm, pH 3–10 nonlinear) and other chemicals for 2D-DIGE, unless otherwise specified, were purchased from Bio-Rad Laboratories Inc. (Hercules, CA, USA).

### Physicochemical characterization

The size distribution of the 25 nm CuNPs suspended in 1% (w/v) HPMC was determined with a dynamic light scattering particle size analyzer (LB-550, Horiba Ltd, Fukuoka, Japan) and atomic force microscopy (Daojin Co., Japan). X-ray diffraction (XRD) was performed using a Bruker D8 Advance X-ray diffractometer with Cu Kα radiation ($\lambda$ = 1.54 Å). The specific surface area was determined with a Brunauer–Emmett–Teller surface area analyzer (ASAP 2020, Micromeritics, Norcross, GA, USA). The impurities (*e.g.*, aluminum, barium, calcium, chromium, chrome, iron, magnesium, manganese molybdenum, and sodium) were identified by X-ray fluorescence spectroscopy. The dissolution of ionic copper from the 25 nm CuNPs in HPMC was measured through inductively coupled plasma-atomic absorption spectrometry (ICP-AAS-7000, Daojin Co., Japan) after 30 min of ultrasonication.

### Animals

All of the animal studies were approved by the Ethics Committee of Animal Care and Experimentation of the National Institute for Environmental Studies, China. Male Wistar rats (200 ± 10 g) were purchased from Weitong-Lihua Experimental Animal Center (Beijing, China) and housed in stainless-steel cages with a 12 h light/dark cycle, ventilated with an air exchange rate of 15 times $h^{-1}$, and maintained at 20–25 °C with a relative humidity of 40–60%. Each animal was allowed free access to water and pellet food. After a seven-day quarantine and acclimatization period, the rats were divided into four groups of six using a computerized stratified random grouping method based on body weight. The rats were administered daily doses of the CuNP suspension (100 or 200 mg $kg^{-1}$), CuMP suspension (200 mg $kg^{-1}$), or 1% HPMC vehicle by oral gavage for five consecutive days (dosing volume of 10 ml $kg^{-1}$, $n$ = 6).

### Body weights, clinical chemistry, and liver and kidney histopathology and ultrastructure analysis

The body weights were measured each day before dosing. After five days of exposure, blood samples were collected from the heart of the animals under ether anesthesia using a needle. The clinical chemistry analysis of the serum samples was carried out with a Hitachi 7020 automatic analyzer using appropriate kits. The following parameters were tested: alanine aminotransferase (ALT), aspartate aminotransferase (AST), alkaline phosphatase (ALP), total protein (TP), albumin (ALB), glucose (GLU), total cholesterol (TCHOL), triglyceride (TG), total bilirubin (TBILI), total bile acid (TBA), blood urea nitrogen (BUN), and creatinine (Crn).

Cross-sections of the livers and kidneys were snap frozen in liquid nitrogen and stored at −80 °C until proteomic analysis. The remaining liver and kidney tissues were fixed in 10% buffered formalin for routine histological processing. Paraffin sections were stained with H&E for histopathological examination. For ultrastructure evaluation, formalin-fixed liver and kidney sections were transferred to phosphate-buffered 2.5% glutaraldehyde and embedded in epoxy resin. Thin sections were collected on copper grids, stained with uranyl acetate and lead citrate, and examined with a transmission electron microscope.

### Copper accumulation analysis—Howell's rubeanic acid stain

Thin (5 μm) paraffin sections of the formalin-fixed livers and kidneys were brought to water using xylene and ethanol and



 

placed in the working rubeanic acid solution overnight at 37 °C. The sections were placed in 70% ethanol for 15 minutes and then in absolute ethanol overnight. Next they were lightly counterstained with alcoholic eosin and rinsed well with absolute ethanol. The sections were cleared with xylene and mounted with a resinous medium. The sections were then inspected for the presence of green-black granules, which signal the presence of intracellular copper.

### 2D DIGE and imaging

Approximately 0.2 g of each of the liver and kidney samples was ground into a fine powder in liquid nitrogen and homogenized in lysis buffer (7 M urea, 2 M thiourea, 4% 3-[(3-cholanidopropyl)dimethylammonio]-1-propanesulfonate [CHAPS], 10 mM Tris, 5 mM magnesium acetate, and one complete protease inhibitor cocktail tablet per 50 ml of lysis buffer) using a 4 ml Potter–Elvehjem homogenizer precooled with ice. Fifty microliters of lysis buffer were used for approximately 100–150 mg of each liver or kidney sample. The samples were centrifuged, and the supernatants were stored at −80 °C. The protein concentration was determined using the Bradford assay kit (Bio-Rad Laboratories, Inc.).

The pH of the protein was adjusted to 8.5 with 50 mM NaOH, and the concentration was adjusted to 5 mg $ml^{-1}$ with lysis buffer. Equal amounts of proteins from the individual control and treated animals were pooled together as the internal standard. The treated and control counterparts of the experimental rats were randomly labeled with Cy3 or Cy5, whereas the internal standards were labeled with Cy2 using 400 pmol of fluorochrome per 50 μg of protein. The labeling was performed for 30 min in the dark. The reactions were then quenched by the addition of 1 μl of lysine (10 mM) for 10 min on ice in the dark.

Fifty micrograms of the Cy3- and Cy5-labeled samples from each rat were combined before mixing with 50 μg of Cy2-labeled internal standard. An equal volume of 2 × sample buffer (7 M urea, 2 M thiourea, 4% CHAPS, 1% Bio-Lyte, pH 3–10, and 20 mg $ml^{-1}$ DTT) was then added to the sample, and the total volume was increased to 410 μl with rehydration buffer (7 M urea, 2 M thiourea, 4% CHAPS, 0.5% Bio-Lyte, and 10 mg $ml^{-1}$ DTT).

The samples were actively rehydrated into 24 cm pH 3–10 IPG strips (Bio-Rad) at 17 °C for 12 h using a Protean IEF cell (Bio-Rad). Isoelectric focusing was performed for a total of 80 kV-h (increased to 250 V in 30 min, maintained at 1000 V for 1 h, increased to 10 000 V in 5 h, and maintained at 10 000 V for 60 kV-h). The IPG strips were equilibrated in equilibration buffer (6 M urea, 2% SDS, 50 mM Tris-Cl, pH 8.8, and 30% glycerol) supplemented with 0.5% DTT for 15 min at room temperature and then incubated with 4.5% iodoacetamide in equilibration buffer for 15 min at room temperature.

The IPG strips were placed on the top of 12% homogeneous polyacrylamide gels that had been precast with low fluorescence glass plates using an Ettan DALT twelve gel caster. The two-dimensional SDS-PAGE was carried out using the Protean Plus system (Bio-Rad). After 2DE, the gels were scanned on a Typhoon 9410 scanner with Ettan DALT gel alignment guides using excitation/emission wavelengths specific for Cy2 (488/520 nm), Cy3 (532/580 nm), and Cy5 (633/670 nm). The intensity was adjusted to ensure that the maximum volume of each image was within 60 000–90 000.

### Data analysis

The 2D DIGE analysis was performed using the DeCyder 5.0 software (GE Healthcare) according to the manufacturer's recommendations. Briefly, the DeCyder biological variation analysis module was used to detect the spots (the estimated number of spots was 2500). All of the matches were also confirmed manually. The paired $t$ test was used for the statistical analysis of the data. The protein spots that were differentially expressed in the treated and control groups (ratio $\geq 2$, $p \leq 0.01$) were marked.

### In-gel digestion

Spot-picking was carried out with preparative gels. Two-dimensional electrophoresis was performed as described above with the exception that the IPG strips were loaded with 500–1000 μg of protein, and the gels were stained with Coomassie Brilliant Blue. The protein spots of interest were excised and destained with 25 mM ammonium bicarbonate/50% acetonitrile (ACN). The gels were then dried completely by centrifugal lyophilization. In-gel digestion was performed with 0.01 g $l^{-1}$ trypsin (Promega Corp., Madison, WI, USA) in 25 mM ammonium bicarbonate for 15 h at 37 °C. The supernatants were collected, and the tryptic peptides were extracted from the gel sequentially with 5% trifluoroacetic acid (TFA) at 40 °C for 1 h and with 2.5% TFA/50% ACN at 30 °C for 1 h. The extracts were pooled and dried completely by centrifugal lyophilization.

### Protein identification

The altered protein spots were manually excised from the 2D gels. The gel pieces were processed using the following successive stages: washing in 25 mM ammonium bicarbonate, dehydration in ACN, hydrolysis in 0.01 μg $\mu l^{-1}$ trypsin, and extraction with ACN. For matrix-assisted laser desorption/ionization-time-of-flight mass spectrometry/time-of-flight mass spectrometry (MALDI-TOF/TOF MS) analysis, 1 μl of the digested mixture was mixed with 0.5 μl of 100 mM α-cyano-4-hydroxy-cinnamic acid in 50% ACN/0.1% TFA on the target plate before being dried and analyzed with a MALDI-TOF/TOF mass spectrometer (MS) (Applied Biosystems 4700 Proteomics Analyzer, Life Technologies Corp., Grand Island, NY, USA). MALDI-TOF MS and TOF-TOF tandem MS were performed. The data were acquired in the positive MS reflector mode with a scan range of 600 to 4000 Da, and the parent ion peaks (minimum S/N > 15) were selected for MS/MS analysis. For interpretation of the mass spectra, a combination of peptide mass fingerprints and peptide fragmentation patterns was used for protein identification in the National Center for Biotechnology Information non-redundant database against all of the entries using the Mascot Server search engine (http://www.matrixscience.com). All of the mass values were considered

monoisotopic, and the peptide tolerances were 75 ppm and 0.2 Da for the MS and MS/MS spectra, respectively. One missed cleavage site was allowed for trypsin digestion; cysteine carbamidomethylation was assumed as a fixed modification, and methionine was assumed to be partially oxidized. The results with CIs greater than 95% were considered positive identifications. The identified proteins were then matched to specific processes or functions by searching the GO database (http://www.geneontology.org).

### Biological information

The subcellular location of the deregulated proteins was determined from the Swiss-Prot knowledgebase (http://www.ebi.ac.uk/swissprot/). The proteins of interest were submitted to GeneGO version 5.4 to obtain their biological function information. The MetaCore module was used to determine their functional ontologies for enrichment analysis. The degree of relevance to different categories for the comparison datasets was defined by *p*-values. In this study, the threshold was 0.001, and the *p*-value threshold was 0.05.

### Western blot analysis

Ten micrograms of the proteins were separated by SDS-PAGE and transferred onto nitrocellulose membranes at 100 V and 4 °C for 75 min using transfer buffer (25 mM Tris, 192 mM glycine, 20% methanol). The membranes were blocked in 5% nonfat, dry milk in Tris-buffered saline with Tween (TBST) (50 mM Tris-HCl, 150 mM NaCl, pH 7.4, 0.1% Tween 20) for 2 h at room temperature and subsequently incubated with primary antibody diluted in blocking buffer for 1 h [(rabbit anti-catalase, AB16731, dilution 1 : 4000) or (mouse anti-RGN, HM3018, dilution 1 : 1000; goat anti-CA3, SC-50714, dilution 1 : 1000; Santa Cruz Biotechnology, CA, USA)] overnight at 4–7 °C. The membranes were incubated at room temperature for 1 h with each primary antibody, washed three times with TBST and incubated with horseradish peroxidase-conjugated secondary antibody (diluted 1 : 10 000, Santa Cruz Biotechnology, CA, USA) for 1 h at room temperature. The visualization of the immunoreactive proteins was accomplished using ECL reagents (Santa Cruz Biotechnology).

### Lipid peroxidation and hydrosulfide assays

**Tissue preparation.** The liver and kidney samples were homogenized in TCA (1 : 20, w/v) for 60 s in plastic conic tubes using a homogenizer driven at 50 000 r $min^{-1}$ for 10 s three times. The homogenates were maintained on ice and centrifuged at 4 °C and 6000*g* for 15 min. The supernatants were separated for further preparation, and biochemical assays of the malondialdehyde (MDA), total thiol (TSH), non-protein thiol (NPSH), and protein thiol (PSH) fractions were performed.

**MDA assay.** The lipid peroxidation measurement was performed according to the literature.[15] One of the major secondary products of lipid peroxidation is MDA, which, along with other byproducts, reacts with thiobarbituric acid to generate a colored product. This product absorbs maximally at 535 nm and represents the color produced by all of the thiobarbituric acid-reactive substances.

**TSH, NPSH, and PSH assays.** The levels of TSH and NPSH were estimated with DTNB according to a previously described method.[16] In this assay, DTNB is reduced to 2-nitro-5-mercaptobenzoic acid by the non-protein sulfhydryl groups present in the TCA extract. The absorbance of the characteristic yellow product was measured at 412 nm. The level of PSH was assumed to be equal to the difference between TSH and NPSH. The protein content was assayed using a previously described method.[17]

**Statistics.** The quantitative variables are expressed as the mean values ± standard deviations. The statistical analyses were performed using the SPSS.13.0 software. The data were introduced into a SPSS.13 database and analyzed through adequate statistical methods. The comparisons were carried out using one-way ANOVA followed by Dunnett's test to evaluate whether the means were significantly different among the groups. A $p$ value less than 0.05 was considered significant. The paired $t$-test was used for the statistical analysis of the data with a $p$ value less than 0.01 (Student's $t$-test) for the selection of differentially modulated protein spots.

## Results

### Physicochemical characterization

The physicochemical characterization results are summarized in Table 1. The dynamic light scattering analysis results indicate that CuNPs could not be dispersed individually following 30 min of ultrasonication in 1% hydroxypropylmethyl cellulose (HPMC) solution, and their mean aggregate size was approximately 90 nm. The dissolution rate of copper ions from the CuNPs in 1% HPMC was 0.014 ± 0.002% (93 ± 13 μg $min^{-1}$) following 30 min of ultrasonication. The X-ray diffraction pattern of the copper nanoparticles showed that only a small fraction of the copper nanoparticles had transformed into cuprous oxide, corresponding to 16.86%.

### Conventional toxicology results

Symptoms of gastrointestinal dysfunction, such as anorexia and severe diarrhea, were observed in all of the rats that received CuNPs (200 mg $kg^{-1}$) for five days. Drowsiness, hypopnea, tremors, and arching of the back were observed in four of the six rats treated with this dose. The rats in this group also exhibited marked weight loss and significantly increased average kidney weight compared with the control group.

**Table 1** Physicochemical parameters of nano-copper and micro-copper

| Particles | Average size | Size distribution | BET surface area ($m^2$ $g^{-1}$) | Purity (%) |
|---|---|---|---|---|
| Nano-copper | 25 nm | 5–60 nm | 6.93 ± 0.03 | 99.9 |
| Micro-copper | 17 μm | 0.5–38 μm | 0.25 ± 0.03 | 99.9 |

No clinical signs of toxicity were observed in the other treated groups and the control group.

Significant changes in the serum clinical biochemistry parameters were restricted to the rats treated with a high dose of CuNPs (200 mg $kg^{-1}$). The abnormalities of the serum biochemistry parameters are illustrated in our previous work[3] and are listed as follows: the levels of aspartate aminotransferase (AST), total bilirubin, blood urea nitrogen (BUN), and creatinine (Crn) in this group were significantly elevated (greater than five-fold) compared with the control group, and the alanine aminotransferase (ALT) level was increased to a lesser extent (greater than two-fold). Additionally, the alkaline phosphatase and total cholesterol levels were significantly reduced, whereas the total protein and triglyceride levels were elevated significantly in the group treated with 200 mg $kg^{-1}$ $d^{-1}$ CuNPs compared with the control group.

The comparison of the hematoxylin- and eosin- (H&E-) stained liver sections from the control and CuNP-treated rats indicated scattered dot hepatocytic necrosis in all of the rats administered CuNPs at a dose of 200 mg $kg^{-1}$ $d^{-1}$ (Fig. 1B). No signs of necrosis were observed in the livers of rats from the group administered 100 mg $kg^{-1}$ $d^{-1}$ CuNPs. Significant damage was also observed in the renal tissues from the CuNP-treated rats, whereas in all of the rats dosed with 200 mg $kg^{-1}$ $d^{-1}$ CuNPs, the changes consisted of widespread renal proximal tubule necrosis involving most of the nephrons. Additionally, cellular fragments were found in the tubule lumen, where orange crystal matter deposition was commonly observed (Fig. 1D). Swelling of the proximal tubule epithelia was the only change observed in the kidneys of the rats dosed with 100 mg $kg^{-1}$ $d^{-1}$ CuNPs.

The transmission electron microscopy (TEM) photographs of thin liver and kidney sections from the rats treated with CuNPs (200 mg $kg^{-1}$) revealed ultrastructural changes in the hepatocytes, including swollen mitochondria, disordered endoplasmic reticula, and deformed nuclei. The changes observed in the renal proximal tubular epithelial cells of the rats in this group consisted of liquescent necrosis and deformed nuclei and nucleoli (Fig. 1F and H).

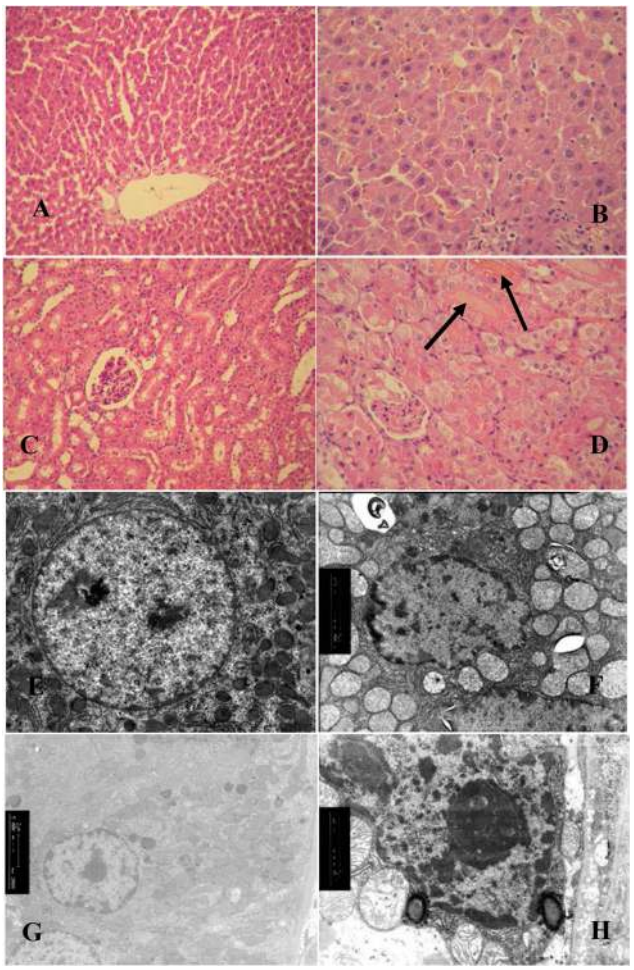


Fig. 1 Histopathological pictures of the rat liver and kidneys. (A), (B), (C), (D) stained with hematoxylin and eosin of rat livers and kidneys in the control (200×) and 200 mg $kg^{-1}$ nano-copper groups (400×). (A) and (C) show normal; (B) exhibits scattered dot hepatocytic necrosis; (D) indicates a widespread proximal tubular cell necrosis, orange crystal matter are noted; (E), (F), (G)and (H) are electron microscope photographs of rat livers and kidneys in the control and 200 mg $kg^{-1}$ nano-copper groups. (E) and (G) show normal ultrastructure of hepatocyte and nephrocyte (5000×, 12 000×). (F) Exhibits the swelling of the mitochondria, the disorder of the endoplasmic reticulum and the deformity of karyon of the hepatocyte (8000×). (H) Indicates the liquescency necrosis of the renal proximal tubular epithelial cell, the deformity of karyon and nucleoli (17 000×).

### Copper accumulation in the rat liver and kidney

Many green-black granules were observed in the hepatocellular, nephric tubule cellular, and nephric tubular cavity tissues from the rats exposed to CuNPs (200 mg $kg^{-1}$), indicating copper overloading in these tissues (Fig. 2C and F). No granules were observed in the liver or kidney from the control rats or the rats treated with either low-dose CuNPs or microcopper.

### Copper particles induced proteome alterations

Mass spectrometry of 39 and 16 modulated spots in the liver tissues from the rats treated with 200 or 100 mg $kg^{-1}$ $d^{-1}$ CuNPs, respectively, led to the identification of 12 and six different proteins with confidence intervals (CIs) greater than 95%. All of the matched proteins came from the NCBI database for rat species (Tables 2 and 3), and these are translationally involved in many processes, including respiratory and energy metabolism, antioxidant defense, lipid metabolism, the urea cycle, and the biosynthesis of creatine. Only three unique proteins (related cytoskeletal protein: keratin, type II cytoskeletal 8 and 18 and calreticulin) were successfully identified in the livers of the rats treated with 200 mg $kg^{-1}$ microcopper.

Similarly, 20 and 14 different highly expressed proteins were identified in the kidneys of rats treated with CuNPs at 200 and 100 mg $kg^{-1}$, respectively (Tables 4 and 5). These proteins are involved in respiratory and energy metabolism, antioxidant defense, intracellular calcium homeostasis, the urea cycle, the biosynthesis of creatine, and cytoskeletal organiz-

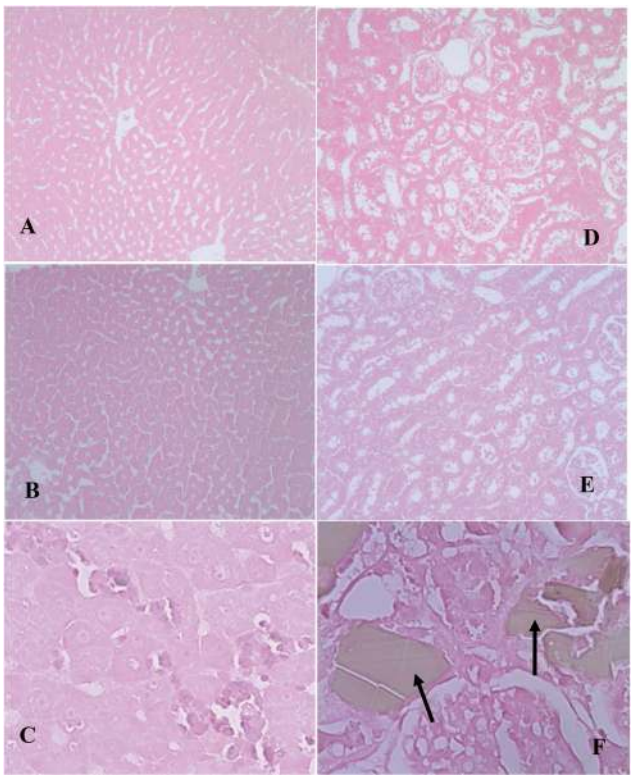


Fig. 2 Howell's rubeanic acid stains of the liver and kidney (A, B, C, liver; D, E, F, kidney). (A, D): Control; (B, E): nano-copper-treated (100 mg $kg^{-1}$ $d^{-1}$) rats (100×); (C, F): nano-copper-treated (200 mg $kg^{-1}$ $d^{-1}$) rats, green-black granules were noted (400×). Green-black granules represent excessive copper ion accumulation in the tissue.

ation. No protein spots were identified in the kidney tissues from the rats treated with 200 mg $kg^{-1}$ microcopper.

### Confirmation of proteomic results

A western blot analysis was performed to confirm four of the post-CuNP-treatment protein expression changes identified using 2D-DIGE. The proteins selected for confirmatory immunoblot analysis were catalase (CAT) and carbonic anhydrase 3 (CA3) in the liver and nicotinamide adenine dinucleotide dehydrogenase [ubiquinone] Fe–S protein 2 (NDUFS2) and regucalcin (RGN) in the kidney. These proteins may be involved in the molecular mechanisms of CuNP toxicity. As shown in Fig. 3, CAT was significantly down-regulated by 2.33-fold in the rats treated with high-dose CuNPs for five days compared with the control rats. CAT expression was decreased 1.56-fold in the low-dose group. RGN was also significantly down-regulated in the rats treated with the low and high doses of CuNPs for five days, with expression ratios of 2.13 and 3.57, respectively, compared with the controls. Consistent with the proteomic results, the western blot analysis showed significant down-regulation of CA3 and NDUFS2 in the kidneys of the rats treated with either the low or high doses of CuNPs for five days.

### Lipid peroxidation in liver and kidney tissues

Significant increases in the levels of malondialdehyde (MDA) were observed in the liver and kidney tissues after the administration of 200 mg $kg^{-1}$ CuNPs compared with the control group (Table 6). In addition, the content of MDA was significantly increased in the livers of the rats treated with100 and

Table 2 Characterization of the identified differentially expressed proteins of rat liver following 200 mg $kg^{-1}$ nano-copper treatment

| Spot id. | Protein identity [gene names], subcellular localization | Accession number | Protein score C.I.% | $M_w$/PI | Molecular function | Fold change |
|---|---|---|---|---|---|---|
| Respiratory and energy metabolism | | | | | | |
| 1746 | Electron transfer flavoprotein subunit beta [Etfb], mitochondria | IPI00364321 | 99.959 | 27 539/7.81 | Electron carrier activity | 2.35 |
| Anti-oxidative defense | | | | | | |
| 563 | Catalase [Cat], peroxisome | IPI00231742 | 100 | 59 588.4/7.15 | Antioxidant activity | −3.18 |
| 1614 | Carbonic anhydrase 3 [Ca3], cytoplasm | IPI00230788 | 100 | 29 281.7/6.97 | Catalyze interconvert carbon dioxide and bicarbonate | −4.05 |
| Phase II metabolic enzymes | | | | | | |
| 1766 | Glutathione *S*-transferase [GST], cytosol, mitochondria | IPI00650116 | 99.928 | 25 552.5/8.89 | Transferase activity | −2.14 |
| 1659 | Glutathione *S*-transferase alpha3 [Gsta3], cytoplasm | IPI00231150 | 100 | 25 971.7/8.98 | Transferase activity | −3.07 |
| 1721 | Glutathione *S*-transferase Mu 1 [Gstm1], cytoplasm | IPI00231639 | 100 | 25 766.1/8.42 | Transferase activity | −2.06 |
| Urea cycle and the biogenesis of creatine | | | | | | |
| 920 | Carbamoyl-phosphate synthase1 [Cps1], mitochondrion | IPI00210644 | 100 | 164 475.5/6.33 | Nitrogen metabolism | −2 |
| 1539 | Glutamate dehydrogenase 1 [Glud1], mitochondria matrix | IPI00324633 | 100 | 61 377.3/8.05 | Nitrogen and glutamate metabolism | 5.82 |
| Other functions related | | | | | | |
| 2020 | Hemoglobin subunit beta-1 [Hbb], red blood cell | IPI00230897 | 100 | 15 838.2/7.98 | Oxygen transport | 4.82 |
| 1667 | Heat shock 70 kDa protein 5 [Hspa5], endoplasmic reticulum lumen | IPI00206624 | 100 | 72 302.4/5.07 | Molecular chaperone | 2.42 |
| 826 | Keratin, type II cytoskeletal 6A [Krt6a], cytoplasm | IPI00393340 | 99.997 | 59 212.7/8.06 | Cytoskeletal | −2.1 |
| 1663 | Keratin, type I cytoskeletal 18 [Krt18], cytoplasm | IPI00480679 | 100 | 47 601.2/5.17 | Cytoskeletal | 2.33 |

Table 3 Characterization of the identified differentially expressed proteins of rat liver following 100 mg $kg^{-1}$ nano-copper treatment

| Spot id. | Protein identity [gene names], subcellular localization | Accession number | Protein score C.I.% | $M_w$/PI | Molecular function | Fold change |
|---|---|---|---|---|---|---|
| Respiratory and energy metabolism | | | | | | |
| 1616 | ATP synthase subunit beta [Atp5b], mitochondrion inner membrane | IPI00551812 | 100 | 56 318.5/5.19 | Electron transport activity | 2.16 |
| 1217 | Alpha-enolase [Eno1], cytoplasm; cell membrane | IPI00464815 | 94.795 | 46 967.2/6.16 | Glycolytic enzyme | 2.5 |
| 1003 | Isocitrate dehydrogenase [NADP] cytoplasmic [Idh1] cytoplasmic | IPI00194045 | 99.972 | 46 704.5/6.53 | Catalyze the oxidative decarboxylation | 1.52 |
| Fatty acid catabolism | | | | | | |
| 800 | Hydroxymethylglutaryl-CoA synthase 2 [Hmgcs2] cytosol; mitochondrion | IPI00210444 | 99.944 | 56 875.6/8.86 | Synthesis of ketone bodies; cholesterol synthesis | 1.72 |
| Urea cycle and the biogenesis of creatine | | | | | | |
| 945 | Argininosuccinate synthase [Ass1], endoplasmic reticulum; mitochondrial outer membrane | IPI00211127 | 100 | 46 466.9/7.63 | Urea and nitric oxide synthesis | −2.98 |
| Other function related | | | | | | |
| 1053 | Heat shock 70 kDa protein 5 [Hspa5], endoplasmic reticulum lumen | IPI00206624 | 100 | 72 302.4/5.07 | Molecular chaperone | 2.51 |

Table 4 Characterization of the identified differentially expressed proteins of rat kidney following 200 mg $kg^{-1}$ nano-copper treatment

| Spot id. | Protein identity [gene names], subcellular localization | Accession number | Protein score C.I.% | $M_w$/PI | Molecular function | Fold change |
|---|---|---|---|---|---|---|
| Respiratory and energy metabolism | | | | | | |
| 806 | NADH dehydrogenase (ubiquinone), iron-sulfur protein 2 [Ndufs2], mitochondrial inner membrane, peripheral membrane protein | IPI00471647 | 100 | 52 527.6/6.52 | Electron carrier activity | −2.89 |
| Anti-oxidative defense | | | | | | |
| 1748 | Glutathione peroxidase 3 [Gpx3] secreted | IPI00476458 | 100 | 25 546/8.2 | Transferase activity | −2.19 |
| Calcium homeostasis | | | | | | |
| 1255 | Regucalcin [Rgn], cytoplasm | IPI00389611 | 99.074 | 33 368.4/5.27 | Calcium-binding protein | −2.68 |
| 1666 | Calbindin [Calb1], cytoplasm | IPI00231118 | 99.98 | 29 844/4.71 | Calcium-binding protein | −2.21 |
| Urea cycle and the biogenesis of creatine | | | | | | |
| 812 | Glycine amidinotransferase, mitochondrial [Gatm], mitochondrial inner membrane | IPI00198444 | 100 | 48 211/7.17 | Arginine and creatine biosynthesis | −2.98 |
| Cytoskeleton proteins | | | | | | |
| 537 | Tubulin beta-5 chain [Tubb5], microtubule | IPI00197579 | 100 | 49 639/4.78 | Cytoskeleton | 3.35 |
| 626 | Tubulin alpha-6 chain [Tuba6], microtubule | IPI00364046 | 100 | 49 905.5/4.96 | Cytoskeleton | 5.12 |
| 577 | Keratin, type II cytoskeletal 8 [Krt8], cytoplasm | IPI00389571 | 94.674 | 53 854.2/5.82 | Cytoskeleton | 12.88 |
| 290 | Spectrin alpha chain [Sptan1], cytoplasm cytoskeleton | IPI00209258 | 99.984 | 284 537.3/5.23 | Actin capping | 10.56 |
| Other functions related | | | | | | |
| 300 | Serum albumin [Alb], secreted protein | IPI00191737 | 100 | 68 674/6.09 | Carrier protein | 9.02 |
| 1975 | Hemoglobin subunit beta-1 [Hbb], red blood cells | IPI00230897 | 100 | 15 838.2/7.98 | Oxygen transport | 12.27 |
| 1314 | L-Lactate dehydrogenase B chain [Ldhb], cytoplasm | IPI00231783 | 100 | 36 458/5.7 | Catalytic activity, oxidoreductase activity | −2.04 |
| 479 | Serine protease inhibitor A3 K [Serpina3k], secreted protein | IPI00200593 | 99.998 | 46 532.1/5.31 | Inhibits kallikreins and trypsin | 4.26 |
| 581 | Serine protease inhibitor A3N [Serpina3n], secreted protein | IPI00211075 | 99.998 | 46 622.3/5.33 | Serine protease inhibitor activity | 11.58 |
| 476 | Disulfide-isomerase [P4hb], endoplasmic reticulum lumen | IPI00198887 | 100 | 56 915.7/4.82 | Catalyze protein folding | 4.68 |
| 201 | Methylcrotonoyl-CoA carboxylase subunit alpha [Mccc1], mitochondrion | IPI00372191 | 99.656 | 79 279.4/6.66 | Leucine degradation | 4.25 |
| 1671 | Triosephosphate isomerase [Tim], cytoplasm | IPI00231767 | 99.975 | 26 772.7/6.51 | Glycolysis pathway | −2.04 |
| 1381 | Proteasome activator complex subunit 2 [Psme2] | IPI00211970 | 99.998 | 26 709/5.52 | Modified proteasome | −2.03 |
| 1809 | Cys2/His2 zinc finger protein [zf-C2H2] | IPI00565417 | 99.596 | 85 346.7/9.4 | Interaction modules | 4.62 |
| 630 | Vitamin D-binding protein precursor, secreted protein | IPI00194097 | 100 | 53 509/5.65 | Binds and transports vitamin D | 6.25 |

200 mg $kg^{-1}$ $d^{-1}$ copper nanoparticles. No significant change in MDA was observed following copper microparticle treatment.

Table 7 summarizes the alterations in the total thiol groups (TSH), non-protein thiol groups (NPSH), and protein thiol groups (PSH) resulting from the CuNP and microcopper treat-

Table 5 Characterization of the identified differentially expressed proteins of rat kidney following 100 mg kg$^{-1}$ nano-copper treatment

| Spot id. | Protein identity [gene names], subcellular localization | Accession number | Protein score C.I.% | $M_w$/PI | Molecular function | Fold change |
|---|---|---|---|---|---|---|
| Respiratory and energy metabolism | | | | | | |
| 872 | ATP synthase subunit beta [Atp5b], mitochondrial inner membrane | IPI00551812 | 100 | 56 318.5/5.19 | Transporter activity | 1.51 |
| 784 | Ubiquinol-cytochrome c reductase core protein 1 [Uqcrc1], mitochondrial inner membrane | IPI00471577 | 99.116 | 52 815.4/5.57 | Transporter activity | 1.86 |
| 1146 | Isocitrate dehydrogenase [NAD] subunit alpha [Idh3a], mitochondrial matrix | IPI00198720 | 99.997 | 39 588/6.47 | Electron carrier activity | 1.76 |
| 1373 | Electron transfer flavoprotein subunit alpha [Etfa], mitochondrial matrix | IPI00205332 | 98.021 | 34 929.5/8.62 | Electron transfer | −1.99 |
| 704 | Dihydrolipoyllysine-residue succinyltransferase component of 2-oxoglutarate dehydrogenase complex [Dlst], mitochondrion | IPI00551702 | 100 | 48 894.4/8.89 | Electron carrier activity | −1.84 |
| Hydration of carbon dioxide | | | | | | |
| 1565 | Carbonic anhydrase 2 [Ca2], cytoplasm | IPI00230787 | 99.983 | 28 964.6/6.88 | Catalyze interconvert carbon dioxide and bicarbonate | 2.42 |
| Calcium homeostasis | | | | | | |
| 1668 | Calbindin [Calb1], cytoplasm | IPI00231118 | 100 | 29 844/4.71 | Calcium-binding protein | −1.54 |
| Urea cycle and the biogenesis of creatine | | | | | | |
| 883 | Argininosuccinate synthase [Ass1], endoplasmic reticulum, mitochondrial outer membrane | IPI00211127 | 100 | 46 466.9/7.63 | Arginine enzyme | −1.61 |
| Other functions related | | | | | | |
| 1026 | Fructose-1,6-bisphosphatase 1, cytoplasm | IPI00231745 | 100 | 39 453.1/5.54 | glyconeogenesis | −1.83 |
| 371 | Serum albumin [Alb], secreted protein | IPI00191737 | 99.99 | 68 674/6.09 | Carrier protein | 3.5 |
| 562 | Tubulin, beta 2c [Tubb2c], cytoplasm | IPI00400573 | 100 | 49 769/4.79 | Cytoskeleton | 1.67 |
| 467 | Vimentin [Vim], cytoplasm | IPI00230941 | 100 | 53 569/5.06 | Cytoskeleton | 3.5 |
| 843 | Zinc finger protein 9 [Azf9] | IPI00763781 | 86.31 | 81 133.6/9.15 | Interaction modules | −1.84 |
| 887 | 4-hydroxyphenylpyruvate dioxygenase [Hppd] | IPI00211507 | 99.987 | 44 952.8/6.29 | Oxygenase enzymes involved L-tyrosine catabolism | −1.58 |

ments. Treatment with 200 mg kg$^{-1}$ d$^{-1}$ CuNPs significantly decreased the NPSH and PSH levels in the livers and kidneys compared with the control group. The magnitude of the decrease in NPSH was greatest in both the liver and kidney, suggesting dose-related down-regulation in the CuNP-treated rats.

## Discussion

In the current study, a series of toxicity manifestations and the conventional toxicology parameters suggested that the rats treated with 200 mg kg$^{-1}$ d$^{-1}$ CuNPs showed much more serious hepato- and nephrotoxicity than those observed in the rats treated with 100 mg kg$^{-1}$ d$^{-1}$ CuNPs. The severity of the hepato- and nephrotoxicity of the rats treated with CuNPs at different doses was not only consistent with the respective copper accumulation in the liver and kidney tissues but also consistent with the results of previous studies on the oral ingestion of excess copper compound. In addition, the toxicity in the rats dosed with copper microparticles was negligible.

A previous study suggested that, compared with the CuMPs, ultrahigh reactivity due to a larger surface area-to-volume ratio per given mass provoked the toxicity of nanocopper *in vivo*. The copper nanoparticles may not affect the mice directly, but may rapidly react with gastric acid after oral exposure, leading to the accumulation of excessive alkalescent substances and copper ions, which can contribute to the acute oral toxicity of the copper nanoparticles.[7] In a recent *in vitro* system, the cellular uptake of copper nanoparticles was confirmed using a transmission electron microscope,[18,19] which suggested that copper nanoparticles can contribute to the intracellular copper overloading. In addition, the copper nanoparticles appeared to target the cell membrane with a rapid loss of membrane integrity and cell death, and the observed membrane damage was caused by the metal release process at the cell membrane surface.[20,21] However, it remains unclear to what extent the hepato- and nephrotoxicity induced by CuNPs can be explained by the soluble copper fraction or by the specific particle. Compared with the copper particles, copper ion can be readily absorbed at the site of the stomach and small intestine, and we hypothesized that the soluble copper fraction released in the gastric acid of the copper particles may predominately contribute to significant copper overloading in the target organs and that it plays an important role in the hepato- and nephrotoxicity of the rats administered the copper nanoparticles.

Through an analysis of the RNA and metabolic profiles, our groups have revealed an unprecedented amount of mechanistic information on the molecular responses and earlier biomarkers involved in the hepato- and nephrotoxicity of the rats treated with copper nanoparticles through a subacute oral exposure protocol.[3,13,14] In addition, the results from this study further testified some changes that provided additional insights into the molecular mechanisms of copper nanoparti-



 

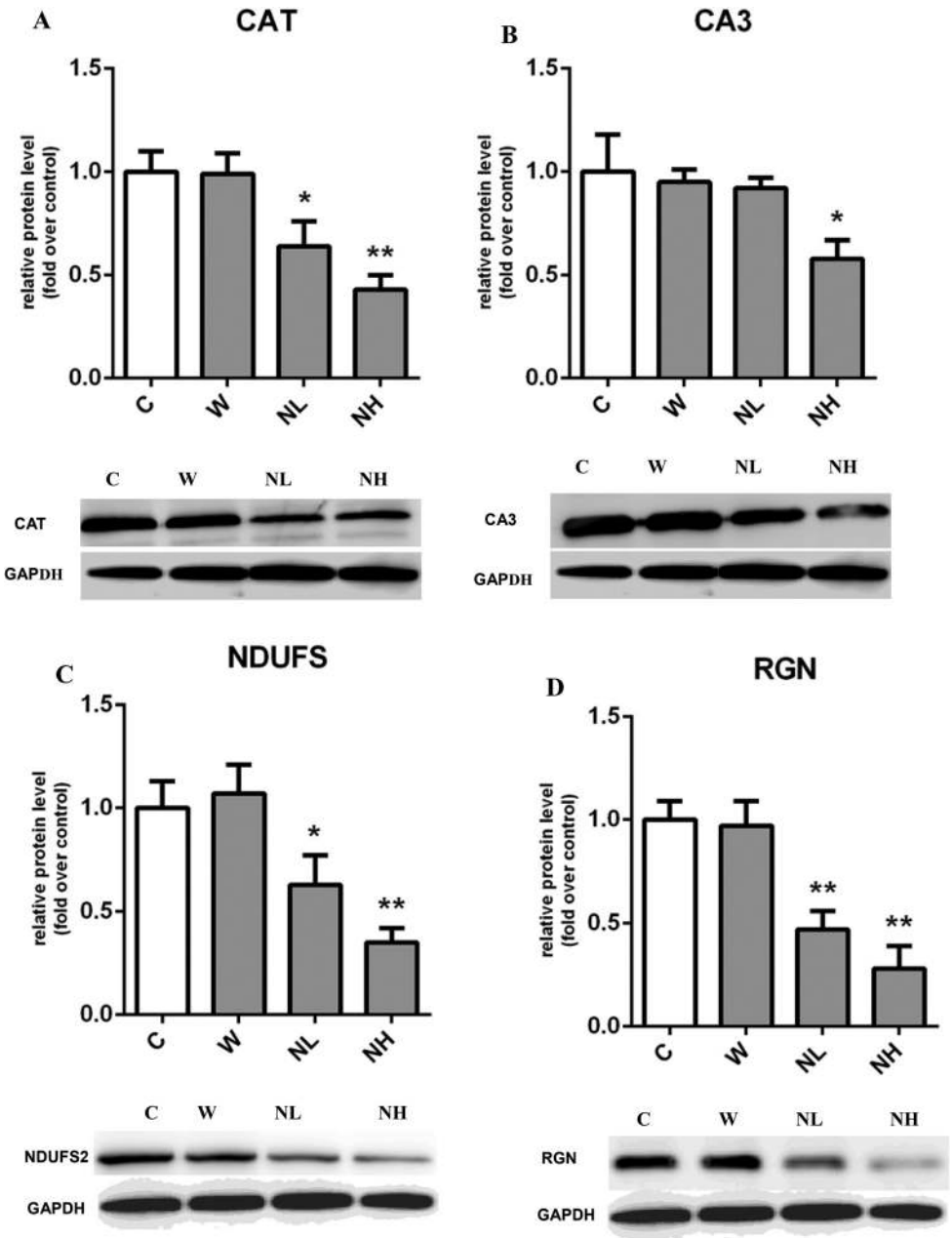


Fig. 3 (A) The protein expression of CAT in the rat liver; (B) the protein expression of CA3 in the rat liver; (C) the protein expression of NDUFS2 in the rat kidney. (D) The protein expression of RGN in the rat kidney. C: control; W: Cu-MP (200 mg/ $kg^{-1}$); NL: Cu-NP (100 mg $kg^{-1}$); NH: Cu-NP (200 mg $kg^{-1}$). Compared with the control group, statistically significant changes are indicated as *$p < 0.05$, **$p < 0.01$ respectively.

Table 6 The content of MDA of rats' livers and kidneys exposed to micro- and nano-copper ($n = 6$, $\bar{x} \pm s$)[a]

| Group | Liver (nmol $mg^{-1}$) | Kidney (nmol $mg^{-1}$) |
|---|---|---|
| Control | 3.18 ± 0.57 | 2.92 ± 0.36 |
| Cu-MP 200 mg $kg^{-1}$ | 3.33 ± 0.17 | 3.21 ± 0.88 |
| Cu-NP 100 mg $kg^{-1}$ | 5.19 ± 0.96* | 3.61 ± 0.68 |
| Cu-NP 200 mg $kg^{-1}$ | 6.31 ± 0.68** | 4.19 ± 0.34* |

[a] Note: Compared with the control group, statistically significant changes are indicated as *$p < 0.05$, **$p < 0.01$ respectively.

cle-induced hepatotoxicity and nephrotoxicity at the protein level.

### Oxidative stress and lipid peroxidation

Previous studies have indicated that the down-regulation of the glutathione metabolism and antioxidant genes contribute to CuNP-induced liver and renal injury.[13,14] Consistent with this finding, using 2D-DIGE technology, down-regulated levels of catalase (fold change −3.18) in the liver and glutathione peroxidase 3 (fold change −2.19) in the kidney were detected in

Table 7 The content of hydrosulfide group of rats' liver and kidney exposed to micro- and nano-copper ($n$ = 6, $\bar{x} \pm s$, μmol $g^{-1}$)[a]

| Groups | Liver | | | Kidney | | |
|---|---|---|---|---|---|---|
| | TSH | NPSH | PSH | TSH | NPSH | PSH |
| Control | 14.45 ± 1.82 | 1.59 ± 0.19 | 12.86 ± 1.63 | 8.74 ± 0.86 | 1.28 ± 0.33 | 7.45 ± 0.77 |
| Cu-MP 200 mg $kg^{-1}$ | 14.17 ± 0.98 | 1.84 ± 0.11 | 12.32 ± 0.98 | 9.33 ± 1.11 | 1.37 ± 0.47 | 7.96 ± 1.156 |
| Cu-NP 100 mg $kg^{-1}$ | 13.68 ± 0.94 | 1.09 ± 0.25* | 12.59 ± 0.76 | 7.64 ± 1.25 | 0.81 ± 0.42 | 6.86 ± 1.02 |
| Cu-NP 200 mg $kg^{-1}$ | 11.74 ± 2.95 | 0.83 ± 0.29** | 10.90 ± 3.03* | 6.55 ± 0.98* | 0.43 ± 0.19* | 6.13 ± 0.94* |

[a] Note: Compared with the control group, statistically significant changes are indicated as $*p < 0.05$, $**p < 0.01$ respectively.

the rats treated with 200 mg $kg^{-1}$ CuNPs. Because it is well known that catalase and glutathione peroxidase 3 can decompose $H_2O_2$ into $H_2O$,[22] their down-regulation hints that the repeated administration of copper nanoparticles weaken the anti-oxidation defense function of the hepato- and nephrocytes of the treated rats. Furthermore, decreased CA3 levels (fold change −4.05) were also observed in the livers of the rats treated with 200 mg $kg^{-1}$ CuNPs. CA3 is a major cytosolic protein, accounting for approximately 8% of the total protein in the rat liver cytosol.[23] It can catalyze the reversible reaction between carbon dioxide and water to form carbonic acid.[24] A previous study suggested that CA3 can play the role of an antioxidant that prevents hydrogen peroxide-inducible apoptosis.[25] Ikeda *et al.* (2000) reported that the marked suppression of CA3 in the rat liver following 3,4,5,3′,4′-pentachlorinated biphenyl (PenCB) treatment could alter the cytosolic pH and lipid metabolism.[26] In addition, oral exposure to CuNPs can lead to the accumulation of excessive alkalescent substances, culminating in metabolic alkalosis.[7] Additionally, oxidative stress damage is the common toxicity mechanism of copper ions and copper nanoparticles. Thus, we hypothesized that the decreased expression of CA3 may contribute to the anti-oxidation and the regulation of the alteration of the cytosolic pH in the liver treated with 200 mg $kg^{-1}$ $d^{-1}$ CuNPs.

Using conventional methods, we further found that prominent decreases in the levels of NPSH and PSH and an increase in the content of MDA were observed in the liver and kidney after exposure to 200 mg $kg^{-1}$ CuNPs. In mammals, low-molecular-weight thiols (in reduced form), such as homocysteine, cysteine, glutathione (GSH), and cysteinylglycine, are collectively referred to as NPSH. GSH constitutes approximately 95% of the cellular NPSH pool.[27] The decreased NPSH levels observed suggest that the first line of defense against oxidative damage was weakened as a result of CuNP exposure. Consistent with this finding, the increase in MDA observed in this study suggests that lipid peroxidation damage had occurred in the target organs. We hypothesized that the overtly accumulated copper ion in the liver and kidney tissue could explain the above alterations induced by repeated exposure to CuNPs.

### Respiratory and energy metabolism

Oral exposure to copper nanoparticles can induce a widespread suppression of mitochondrial oxidative phosphorylation (OxPhos) in the kidney tissues of rats at the transcriptional level. In addition, this damage is associated with reduced activities of complexes I and V of the OxPhos pathway, which translates into a diminished capacity of the renal mitochondria to utilize oxygen and produce ATP from ADP.[14] In this work, the levels of ATP synthase subunit β were increased in the liver (fold change 2.16) and kidney (fold change 1.51), and the expression of the protein ubiquinol-cytochrome c reductase core protein 1 (fold change 1.86) was up-regulated in the kidney in the rats exposed to a low dose of CuNPs. These proteins are components of the ubiquinol-cytochrome c reductase complex (complex III or cytochrome b-c1 complex), which is part of the mitochondrial respiratory chain. Because only slight damage occurred in the rats treated with 100 mg $kg^{-1}$ CuNPs, we hypothesized that the increased expression levels of these proteins may boost the respiratory metabolism and increase ATP production, counteracting the copper accumulation in the livers and kidneys.

Additionally, increased expression levels of α-enolase (fold change 2.5) and isocitrate dehydrogenase [NADP] cytoplasmic (fold change 1.52) in the liver and of isocitrate dehydrogenase NAD subunit alpha (fold change 1.76) in the kidney were observed in the rats treated with 100 mg $kg^{-1}$ copper nanoparticles. Isocitrate dehydrogenase [NADP] cytoplasmic is an enzyme that catalyzes the oxidative decarboxylation of isocitrate to produce α-ketoglutarate and carbon dioxide. It plays a significant role in cytoplasmic nicotinamide adenine dinucleotide phosphate (NADPH) production. NAD(+)-dependent isocitrate dehydrogenases catalyze the allosterically regulated rate-limiting step of the TCA cycle. α-Enolase is a glycolytic enzyme expressed in most tissues that catalyzes the dehydration of 2-phosphoglycerate to phosphoenolpyruvate. The up-regulated expression of these proteins may suggest that glycolysis was intensified to meet the liver cell energy requirements.

In the rats treated with 200 mg $kg^{-1}$ CuNPs, significantly decreased expression levels of NDUFS2 (fold change −2.98) in the kidney were confirmed through 2D-DIGE and western blot analyses. NDUFS2 is a core subunit of the mitochondrial membrane respiratory chain NADH dehydrogenase (complex I) that is believed to belong to the minimal assembly required for catalysis. Complex I functions in the transfer of electrons from NADH to the respiratory chain and catalyzes NADH oxidation with concomitant ubiquinone reduction and proton ejection from the mitochondria. The down-regulation of this protein indicates a diminished capacity of the renal mitochondria to



 

utilize oxygen and produce ATP from adenosine diphosphate. These changes suggest that the widespread renal proximal tubule necrosis induced by 200 mg $kg^{-1}$ CuNPs is related to energy deficiency. Because mitochondria are the preferential target of oxidative injury, we deduced that excessive copper accumulation in the hepato- or nephrocytes would inevitably result in mitochondrial failure and cell death. In contrast, mitochondria are the powerhouses of most cells and produce more than 90% of cellular energy by oxidative phosphorylation. The occurrence of mitochondrial failure would inevitably initiate cell necrosis and delay copper clearance from kidney tissues.

### Phase II metabolic enzymes

Consistent with the decreased NPSH, the levels of glutathione *S*-transferase (GST, fold change −2.14), glutathione *S*-transferase alpha 3 (GSTA3, fold change −3.07), and glutathione *S*-transferase Mu 1 (GSTM1, fold change −2.06) were down-regulated in the livers from the rats treated with 200 mg $kg^{-1}$ CuNPs. GSTs, which are known as ligandins, comprise a family of eukaryotic and prokaryotic phase II metabolic enzymes best known for their ability to catalyze the conjugation of the reduced form of glutathione to xenobiotic substrates for the purpose of detoxification, thereby preventing the interaction of xenobiotics with crucial cellular proteins and nucleic acids.[28,29] GSTA3 and GSTM1 are cytosolic GSTs. A decreased activity of GST in the rat has previously been shown to be a valid marker of hepatotoxicity.[30] We deduced that the down-regulation of these proteins is associated with the lack of a sulfhydryl group supply and also reflects the occurrence of hepatocyte damage after CuNP treatment.

### Calcium homeostasis

In the current work, a significant down-regulation of the expression of proteins involved in the maintenance of calcium homeostasis was detected in the rat kidneys following CuNP treatment at the dose levels of 100 and 200 mg $kg^{-1}$. The proteins include RGN (fold change −2.68) and calbindin (fold change −2.21). The down-regulation of RGN in the kidney was further confirmed by western blot analysis. RGN is predominantly expressed in the liver and kidney cortex, including kidney proximal tubular epithelial cells.[31] This protein has been shown to be involved in the regulation of calcium homeostasis in the kidney proximal tubular epithelial cells,[32,33] which participate in transcellular transport for the reabsorption of calcium from filtered urinary calcium. In addition, RGN has also been shown to regulate various enzyme activities, including calcium-dependent protein kinases and phosphatases, nitric oxide synthase, and cyclic adenosine monophosphate phosphodiesterase, which are involved in intracellular signaling pathways.[34] The kidney RGN expression has also been shown to be down-regulated in renal disorders induced by various drugs. Decreased RGN expression in kidney cells may play a pathophysiological role in the development of renal disorders.[35,36] Compared with RGN, calbindin is an intracellular calcium-binding protein that plays an important role in calcium transport. Functionally, it has been shown that calbindin increases calcium uptake in the distal tubule *in vitro*.[37] Steiner *et al.* (1996) reported that cyclosporine A decreases calbindin-D28k in the rat kidney, as determined by 2D gel electrophoresis.[38] To the best of our knowledge, this study provides the first demonstration of the effect of CuNPs on the kidney calcium-regulation protein levels. We hypothesized that this alteration suggests that disturbed calcium homeostasis may be an important event for the renal adverse effects induced by copper nanoparticles.

### Urea cycle and the biogenesis of creatine

In agreement with the traditional toxicology findings, we observed the following marked alterations of enzymes participating in the urea cycle and the biogenesis of creatine in the rats treated with CuNPs: the rats treated with the high dose of CuNPs presented a down-regulated level of carbamoyl-phosphate synthase 1 (CPSI, fold change −2.0) and an up-regulated level of glutamate dehydrogenase (GLDH, fold change 5.82) in the livers and a down-regulated level of glycine amidinotransferase (AGAT, fold change −2.98) in the kidneys. Among these, CPSI is a mitochondrial ligase enzyme involved in the production of urea and plays a vital role in protein and nitrogen metabolism. After ammonia has been introduced into the mitochondria *via* glutamine or glutamate, CPSI adds the ammonia to bicarbonate along with a phosphate group to form carbamoyl phosphate, which is converted to urea through the urea cycle. Urea can then be transferred back to the blood stream, to the kidneys for filtration and ultimately to the bladder for excretion. The down-regulated CPSI expression could decrease the conversion of ammonia to urea, thus leading to excess ammonia build-up in the body, which would contribute to the toxicity manifestation of the treated rats. Glycine amidinotransferase (AGAT) is a mitochondrial protein involved in the urea cycle and the biogenesis of creatine. Through a proteomic analysis of nephrotoxic compounds inducing proximal tubule damage, Matheis *et al.* (2011) reported that AGAT may be a general marker of proximal tubule damage and is markedly down-regulated.[39] Because a down-regulation of AGAT was found in the proteomic analysis of nephrotoxic compounds inducing proximal tubule damage,[40] its deregulation was consistent with the proximal tubule damage in the rats treated with the high dose of CuNPs.

Glutamate dehydrogenase (GLDH), similarly to ALT, is a relatively liver-specific enzyme;[41,42] however, its intracellular distribution is different. ALT is cytosolic in origin, whereas GLDH is located in the mitochondrial matrix. The remote intracellular concentration of GLDH in the mitochondrial matrices of hepatocytes and its large size (330 kDa) delay its release in cells, leading to cell damage and make it a more specific marker of necrosis.[43] This finding further supported the hypothesis that CuNP-induced hepatocytic necrosis is related to mitochondrial damage.

In addition to the above-mentioned proteins, argininosuccinate synthetase was found to be decreased in the liver (fold

change −2.98) and kidney (fold change−1.61) after treatment with 100 mg $kg^{-1}$ CuNPs. Argininosuccinate synthetase is involved in the synthesis of creatine, polyamines, arginine, urea, and nitric oxide. The transformation of citrulline into argininosuccinate is the rate-limiting step in arginine synthesis. The activity of argininosuccinate synthetase in arginine synthesis occurs largely at the outer mitochondrial membrane of periportal liver cells as part of the urea cycle, with some activity occurring in cortical kidney cells.[44,45] Because only minor hepato- and nephrotoxicity was induced by 100 mg $kg^{-1}$ $d^{-1}$ CuNPs, we hypothesized that the alteration in the expression of argininosuccinate synthetase may reflect a slight dysfunction of the mitochondria.

### Fatty acid catabolism

Up-regulation of hydroxymethylglutaryl-CoA synthase 2 (HMG-CoA; fold change 1.72) was measured in the livers from rats treated with 100 mg $kg^{-1}$ CuNPs. In molecular biology, HMG-CoA is an intermediate in both cholesterol synthesis and ketogenesis and catalyzes the reaction in which acetyl-CoA condenses with acetoacetyl-CoA to form HMG-CoA.[46] In the present study, only a slight increase in the serum cholesterol and triglyceride levels were observed in the low-dose-CuNP-treated group and a previous metabolomic analysis also indicated that CuNPs can induce an increase in triglycerides in the serum, liver and kidney tissues. Thus, we hypothesized that an up-regulation in HMG-CoA expression may have contributed to the lipidosis induced by nanocopper.

### Cytoskeleton proteins

The cytoskeleton-related proteins tubulin beta-5 chain (fold change 3.35), tubulin alpha-6 chain (fold change 5.12), keratin type II cytoskeletal 8 (fold change 12.88), and spectrin alpha chain (fold change 10.56) were significantly up-regulated in the kidneys of rats treated with high-dose CuNPs for five days. Tubulin is the major constituent of microtubules, and cytoskeletal keratins are important intermediate filament proteins that maintain normal signal transduction and protect cells from stress damage, which may result in cell death. Spectrin alpha chain appears to be involved in secretion, interacts with calmodulin in a calcium-dependent manner and is thus likely involved in the calcium-dependent movement of the cytoskeleton at the cell membrane. Under normal conditions, in addition to providing the cell with support and structure, the cytoskeleton is important for cellular motility, intracellular transport, and cellular division. The modulation of actin isoform expression within the same tissue is an important marker of adaptive and/or pathological changes.[47] The up-regulation of these cytoskeleton-related proteins may contribute to the disorder of cellular function. Further studies are needed to clarify the putative role of the up-regulation of cytoskeleton proteins in CuNP-induced nephrotoxicity.

### Hemoglobin subunit beta-1

In addition to mechanism-related proteins, changes in the expression of a protein involved in the resulting hepato- and nephrotoxicity were also identified: hemoglobin subunit beta-1 was up-regulated in the liver (fold change 4.82) and kidney (fold change 12.27) in the rats treated with 200 mg $kg^{-1}$ CuNPs. Hemolysis is one special manifestation after acute or chronic copper toxicity. In short, copper builds up in the liver until a critical concentration is reached, and the resulting liver failure results in a massive release of copper into the blood. The resulting hemolysis causes hemoglobinemia, which produces tubular nephrosis and gun metal-colored kidneys. As a result, the health of the renal tubules could be mediated by the effects of hemoglobin.

## Conclusions

Our study found that the repeated oral administration of CuNPs, but not of microcopper, induced toxicity in rats at the dose of 200 mg $kg^{-1}$ $d^{-1}$, as demonstrated by body weight loss, significant changes in the clinical chemistry parameters, scattered dot hepatocytic necrosis, and widespread renal proximal tubule necrosis. The proteomic analysis results suggested that mitochondrial dysfunction and oxidative damage maybe the initial events in the hepato- and nephrotoxicity of CuNPs. The down-regulation of phase II metabolic enzymes in the liver and the decreased level of calcium-binding protein in the kidney appear to be the specific modes of toxicity in these target organs. The results from this study provide new insights into the hepato- and nephrotoxicity of CuNPs and illustrate how proteomic analyses can provide mechanistic information on the molecular responses to CuNPs.

## Conflict of interest

None declared.

## Acknowledgements

The authors acknowledge the funding support from the Natural Science Foundation (81001254) and the National Foundation (no. 2013ZX09302303).

## References

1 G. Liu, X. Li, B. Qin, D. Xing, Y. Guo and R. Fan, Investigation of the mending effect and mechanism of copper nano-particles on a tribologically stressed surface, *Tribol. Lett.*, 2004, **17**, 961–966.

2 N. Cioffi, N. Ditaranto, L. Torsi, R. Picca, L. Sabbatini, A. Valentini, L. Novello, G. Tantillo, T. Bleve-Zacheo and P. Zambonin, Analytical characterization of bioactive fluoropolymer ultra-thin coatings modified by copper nanoparticles, *Anal. Bioanal. Chem.*, 2005, **381**, 607–616.

3 R. Lei, C. Wu, B. Yang, H. Ma, C. Shi, Q. Wang, Q. Wang, Y. Yuan and M. Liao, Integrated metabolomic



 

analysis of the nano-sized copper particle-induced hepatotoxicity and nephrotoxicity in rats: A rapid *in vivo* screening method for nanotoxicity, *Toxicol. Appl. Pharmacol.*, 2008, **232**, 292–301.
4 Z. Chen, H. Meng, G. Xing, C. Chen, Y. Zhao, G. Jia, T. Wang, H. Yuan, C. Ye and F. Zhao, Acute toxicological effects of copper nanoparticles *in vivo*, *Toxicol. Lett.*, 2006, **163**, 109–120.
5 R. J. Griffitt, R. Weil, K. A. Hyndman, N. D. Denslow, K. Powers, D. Taylor and D. S. Barber, Exposure to copper nanoparticles causes gill injury and acute lethality in zebrafish (Daniorerio), *Environ. Sci. Technol.*, 2007, **41**, 8178–8186.
6 K. Midander, P. Cronholm, H. L. Karlsson, K. Elihn, L. Möller, C. Leygraf and I. O. Wallinder, Surface Characteristics, Copper Release, and Toxicity of Nano-and Micrometer-Sized Copper and Copper(II) Oxide Particles: A Cross-Disciplinary Study, *Small*, 2009, **5**, 389–399.
7 H. Meng, Z. Chen, G. Xing, H. Yuan, C. Chen, F. Zhao, C. Zhang and Y. Zhao, Ultrahigh reactivity provokes nanotoxicity: explanation of oral toxicity of nano-copper particles, *Toxicol. Lett.*, 2007, **175**, 102–110.
8 B. M. Prabhu, S. F. Ali, R. C. Murdock, S. M. Hussain and M. Srivatsan, Copper nanoparticles exert size and concentration dependent toxicity on somatosensory neurons of rat, *Nanotoxicology*, 2010, **4**, 150–160.
9 J. M. Pettibone, A. Adamcakova-Dodd, P. S. Thorne, P. T. O'Shaughnessy, J. A. Weydert and V. H. Grassian, Inflammatory response of mice following inhalation exposure to iron and copper nanoparticles, *Nanotoxicology*, 2008, **2**, 189–204.
10 P. Xu, J. Xu, S. Liu and Z. Yang, Nano copper induced apoptosis in podocytes via increasing oxidative stress, *J. Hazard. Mater.*, 2012, **241–242**, 279–286.
11 W. Slikker, M. G. Paule, L. K. Wright, T. A. Patterson and C. Wang, Systems biology approaches for toxicology, *J. Appl. Toxicol.*, 2007, **27**, 201–217.
12 A. Ng, B. Bursteinas, Q. Gao, E. Mollison and M. Zvelebil, Resources for integrative systems biology: from data through databases to networks and dynamic system models, *Briefings Bioinf.*, 2006, **7**, 318–330.
13 B. Yang, Q. Wang, R. Lei, C. Wu, C. Shi, Y. Yuan, Y. Wang, Y. Luo, Z. Hu and H. Ma, Systems toxicology used in nanotoxicology: mechanistic insights into the hepatotoxicity of nano-copper particles from toxicogenomics, *J. Nanosci. Nanotechnol.*, 2010, **10**, 8527–8537.
14 M. Liao and H. Liu, Gene expression profiling of nephrotoxicity from copper nanoparticles in rats after repeated oral administration, *Environ. Toxicol. Pharmacol.*, 2012, **34**, 67–80.
15 H. Okawa, N. Ohishi and K. Yagi, Assay for lipid peroxides in animal tissues by thiobarbituric acid reaction, *Anal. Biochem.*, 1979, **95**, 351–358.
16 J. Sedlak and R. H. Lindsay, Estimation of total, protein-bound, and nonprotein sulfhydryl groups in tissue with Ellman's reagent, *Anal. Biochem.*, 1968, **25**, 192–205.
17 O. H. Lowry, N. J. Rosebrough, A. L. Farr and R. J. Randall, Protein measurement with the Folin phenol reagent, *J. Biochem.*, 1951, **193**, 265–275.
18 S. Minocha and R. J. Mumper, Effect of Carbon Coating on the Physico-chemical Properties and Toxicity of Copper and Nickel Nanoparticles, *Small*, 2012, **8**, 3289–3299.
19 F. Li, C. Lei, Q. Shen, L. Li, M. Wang, M. Guo, Y. Huang, Z. Nie and S. Yao, Analysis of copper nanoparticles toxicity based on a stress-responsive bacterial biosensor array, *Nanoscale*, 2013, **5**, 653–662.
20 B. A. VanWinkle, K. L. de Mesy Bentley, J. M. Malecki, K. K. Gunter, I. M. Evans, A. Elder, J. N. Finkelstein, G. Oberdörster and T. E. Gunter, Nanoparticle (NP) uptake by type I alveolar epithelial cells and their oxidant stress response, *Nanotoxicology*, 2009, **3**, 307–318.
21 P. Cronholm, K. Midander, H. L. Karlsson, K. Elihn, I. O. Wallinder and L. Möller, Effect of sonication and serum proteins on copper release from copper nanoparticles and the toxicity towards lung epithelial cells, *Nanotoxicology*, 2011, **5**, 269–281.
22 M. C. Paes, M. B. Oliveira and P. L. Oliveira, Hydrogen peroxide detoxification in the midgut of the blood-sucking insect, Rhodniusprolixus, *Arch. Insect Biochem. Physiol.*, 2001, **48**, 63–71.
23 A. Shiels, S. Jeffery, I. R. Phillips, E. A. Shephard, C. A. Wilson and N. D. Carter, Sexual differentiation of rat liver carbonic anhydrase III, *Biochim. Biophys. Acta, Gen. Subj.*, 1983, **760**, 335–342.
24 R. P. Henry, Multiple roles of carbonic anhydrase in cellular transport and metabolism, *Annu. Rev. Physiol.*, 1996, **58**, 523–538.
25 S. R. Räisänen, P. Lehenkari, M. Tasanen, P. Rahkila, P. L. Härkönen and H. K. Väänänen, Carbonic anhydrase III protects cells from hydrogen peroxide-induced apoptosis, *FASEB J.*, 1999, **13**, 513–522.
26 M. Ikeda, Y. Ishii, H. Kato, D. Akazawa, M. Hatsumura, T. Ishida, K. Matsusue, H. Yamada and K. Oguri, Suppression of carbonic anhydrase III in rat liver by a dioxin-related toxic compound, coplanar polychlorinated biphenyl, 3, 3′, 4, 4′, 5-pentachlorobiphenyl, *Arch. Biochem. Biophys.*, 2000, **380**, 159–164.
27 A. Bilska-Wilkosz, M. Ochenduszka, M. G. Iciek, Z. Srebro and L. Włodek, Effects of acetylsalicylic acid on the levels of sulfane sulfur and non-protein sulfhydryl groups in mouse tissues, *Pharmacol. Rep.*, 2013, **65**, 173–178.
28 P. D. Josephy, Genetic variations in human glutathione transferase enzymes: significance for pharmacology and toxicology, *Hum. Genomics Proteomics*, 2010, **2**, 876940.
29 J. D. Hayes, J. U. Flanagan and I. R. Jowsey, Glutathione transferases, *Annu. Rev. Pharmacol. Toxicol.*, 2005, **45**, 51–88.
30 P. S. Giffen, C. R. Pick, M. A. Price, A. Williams and M. J. York, Alpha-glutathione S-transferase in the assessment of hepatotoxicity—its diagnostic utility in comparison with other recognized markers in the Wistar Han rat, *Toxicol. Pathol.*, 2002, **30**, 365–372.

31 M. Yamaguchi and M. Isogai, Tissue concentration of calcium-binding protein regucalcin in rats by enzyme-linked immunoadsorbent assay, *Mol. Cell. Biochem.*, 1993, **122**, 65–68.
32 M. Yamaguchi, Effect of calcium-binding protein regucalcin on Ca2+ transport system in rat liver nuclei: stimulation of Ca2+ release, *Mol. Cell. Biochem.*, 1992, **113**, 63–70.
33 H. Takahashi and M. Yamaguchi, Activating effect of regucalcin on (Ca2+-Mg2+)-ATPase in rat liver plasma membranes: relation to sulfhydryl group, *Mol. Cell. Biochem.*, 1994, **136**, 71–76.
34 M. Yamaguchi, Role of regucalcin in maintaining cell homeostasis and function (review), *Int. J. Mol. Med.*, 2005, **15**, 371–390.
35 H. Misawa and M. Yamaguchi, Involvement of nuclear factor-I (NF1) binding motif in the regucalcin gene expression of rat kidney cortex: The expression is suppressed by cisplatin administration, *Mol. Cell. Biochem.*, 2001, **219**, 29–37.
36 A. Chiusolo, R. Defazio, A. Casartelli, N. Bocchini, M. Mongillo, E. Zanetti, P. Cristofori and A. Trevisan, Regucalcin down-regulation in rat kidney tissue after treatment with nephrotoxicants, *Toxicol. Lett.*, 2008, **182**, 84–90.
37 D. S. Margolis, D. Kim, J. A. Szivek, L.-W. Lai and Y.-H. H. Lien, Functionally improved bone in calbindin-D28k knockout mice, *Bone*, 2006, **39**, 477–484.
38 S. Steiner, L. Aicher, J. Raymackers, L. Meheus, R. Esquer-Blasco, N. L. Anderson and A. Cordier, Cyclosporine A decreases the protein level of the calcium-binding protein calbindin-D 28 kDa in rat kidney, *Biochem. Pharmacol.*, 1996, **51**, 253–258.
39 K. A. Matheis, E. Com, J.-C. Gautier, N. Guerreiro, A. Brandenburg, H. Gmuender, A. Sposny, P. Hewitt, A. Amberg and O. Boernsen, Cross-study and cross-omics comparisons of three nephrotoxic compounds reveal mechanistic insights and new candidate biomarkers, *Toxicol. Appl. Pharmacol.*, 2011, **252**, 112–122.
40 R. P. Amin, A. E. Vickers, F. Sistare, K. L. Thompson, R. J. Roman, M. Lawton, J. Kramer, H. K. Hamadeh, J. Collins and S. Grissom, Identification of putative gene based markers of renal toxicity, *Environ. Health Perspect.*, 2004, **112**, 465.
41 R. Clampitt, An investigation into the value of some clinical biochemical tests in the detection of minimal changes in liver morphology and function in the rat, *Arch. Toxicol. Suppl.*, 1978, **1**, 1–13.
42 J. Lindena, U. Sommerfeld, C. Höpfel and I. Trautschold, Catalytic enzyme activity concentration in tissues of man, dog, rabbit, guinea pig, rat and mouse, Approach to a quantitative diagnostic enzymology, III. Communication, *Clin. Chem. Lab. Med.*, 1986, **24**, 35–48.
43 E. S. Schmidt and F. W. Schmidt, Glutamate dehydrogenase: biochemical and clinical aspects of an interesting enzyme, *Clin. Chim. Acta*, 1988, **173**, 43–55.
44 R. J. Haines, L. C. Pendleton and D. C. Eichler, Argininosuccinate synthase: at the center of arginine metabolism, *Int. J. Biochem. Mol. Biol.*, 2011, **2**, 8.
45 A. Husson, C. Brasse-Lagnel, A. Fairand, S. Renouf and A. Lavoinne, Argininosuccinate synthetase from the urea cycle to the citrulline–NO cycle, *Eur. J. Biochem.*, 2003, **270**, 1887–1899.
46 S. Ohguchi, H. Ichimiya, A. Yagi, H. Hayashi and N. Sakamoto, Copper-induced hypercholesterolemia of golden hamsters: enhanced synthesis of cholesterol in the liver, *Gastroenterol. Jpn.*, 1988, **23**, 629–632.
47 C. Chaponnier and G. Gabbiani, Pathological situations characterized by altered actin isoform expression, *J. Pathol.*, 2004, **204**, 386–395.



 